MATERIALS & DESIGN
VOLUME 61, SEPTEMBER 2014, PAGES 203–210
DOI: 10.1016/J.MATDES.2014.04.052
http://www.sciencedirect.com/science/article/pii/S0261306914003276

FACTORS DETERMINING THE PERFORMANCE OF THERMOPLASTIC POLYMER/WOOD COMPOSITES; THE LIMITING ROLE OF FIBER FRACTURE

Gábor Faludi[1,2], Zoltán Link[1,2], Károly Renner[1,2,*], János Móczó[1,2] and Béla Pukánszky[1,2]

[1]Laboratory of Plastics and Rubber Technology, Budapest University of Technology and Economics, H-1521 Budapest, P.O. Box 91, Hungary

[2]Institute of Materials and Environmental Chemistry, Research Centre for Natural Sciences, Hungarian Academy of Sciences, H-1525 Budapest, P.O. Box 17, Hungary

*Corresponding author: Phone: +36-1-463-2967, Fax: +36-1-463-3474, Email: krener@mail.bme.hu

ABSTRACT

Thermoplastic polymer/lignocellulosic fiber composites were prepared with a considerable range matrices and fibers in an internal mixer. Tensile properties were determined on bars cut from compression molded plates. Local deformation processes initiated around the fibers were followed by acoustic emission testing supported by electron and polarization optical microscopy. The analysis of results proved that micromechanical deformation processes initiated by the fibers determine the performance of the composites. Debonding usually leads to the decrease of composite strength, but decreasing strength is not always associated with poor adhesion and debonding. The direction of property change with increasing wood content depends on component properties and interfacial adhesion. Good interfacial adhesion often results in the fracture of the fibers. Depending on their size and aspect ratio fibers may fracture parallel or perpendicular to their axis. At good adhesion the maximum strength achieved for a particular polymer/wood pair depends on the inherent strength of the fibers, which is larger for perpendicular than parallel fracture. Inherent fiber strength effective in a composite depends also on particle size, larger particles fail at smaller stress, because of the larger number of possible flaws in them. A very close correlation exists between the initiation stress of the dominating local deformation process and composite strength proving that these processes lead to the failure of the composite and determine its performance.

HIGHLIGHTS

- Good interfacial adhesion of components often results in the fracture of fibers.
- Inherent strength of wood flour influences strength and performance of composites.
- Close correlation between initiation of deformation process and composite strength.

Keywords: biocomposites, micromechanical deformations, acoustic emission testing, interfacial adhesion, fiber fracture, inherent strength of wood particles

1. INTRODUCTION

The interest in thermoplastic polymer/wood composites increased significantly in

the last few decades, but also the production and use of these materials grew with a considerable rate [1,2]. Mostly commodity plastics are applied as matrix materials for the production of wood/plastic composites (WPC) [2-4], but PLA is utilized more and more often to produce compostable biocomposites [5-11]. WPCs are often applied in structural applications thus the stiffness and strength of these materials is of large importance [2,12-14]. Stiffness usually increases upon the addition of wood fibers [15-20], but strength may decrease [17,19,21,22] or increase [15,16,18-20] depending on component properties (matrix, fiber) and interfacial interaction. The ultimate goal of reinforcement is to increase or at least preserve strength at the largest value possible.

Polymer/wood composites are heterogeneous materials, thus external load generates inhomogeneous stress distribution around the particles in them [23]. Local stress maxima initiate local micromechanical processes, which influence, in fact often determine the deformation and failure mechanism of the material. A wide variety of such processes were shown to occur in WPCs from the yielding of the matrix to debonding and fiber fracture [10,24-28]. The dominating mechanism determines the composition dependence of most properties and the final performance of the composite. Accordingly, the identification and control of these processes would allow finding ways to improve properties and/or to adjust them to the intended application.

In some of our earlier work we studied micromechanical processes and performance of WPCs prepared with a particular matrix, either various PP polymers [24,25] or PLA [29,30]. We found that the composition dependence of strength depended very much on the specific system studied, e.g. strengths from 7 to 38 MPa were measured in PP composites and close to 50 in PLA at 40-50 vol% fiber content. The decrease or increase of strength could be related to the dominating micromechanical deformation process, but the mechanism itself did not determine the direction of property change. In several cases, usually when the adhesion between the phases was strong, we concluded that the dominating mechanism is the fracture of wood particles [24,25,30,31]. This assumption was supported mainly by SEM micrographs recorded on fracture surfaces created in tensile testing, but such evidence is not sufficiently conclusive. The goal of this paper is to analyze the micromechanical deformation processes in WPCs prepared with diverse matrices. We intended to check the assumption that the wood fractures during deformation and its inherent

strength influences the strength and performance of the composites. We also wanted to identify other factors, if there are any, which might influence composite strength.

2. EXPERIMENTAL

Various polymers were used as matrices in the composites. The PLA (Ingeo 4032 D, M_n = 88500 g/mol, M_w/M_n = 1.8, melt flow rate, MFR = 3.9 g/10 min at 190 °C and 2.16 kg) was acquired from NatureWorks, USA, and it is recommended for extrusion. The three PP polymers were supplied by TVK, Hungary. One was a homopolymer (hPP, Tipplen H 543, M_n = 68700 g/mol, M_w/M_n = 4.16, MFR = 4.0 g/10 min), another a heterophase (bPP, Tipplen K 948, M_n = 38450 g/mol, M_w/M_n = 3.80, MFR = 45.0 g/10 min) and the third a random copolymer (rPP, Tipplen R 359, M_n = 56600 g/mol, M_w/M_n = 3.46, MFR = 12.0 g/10 min). The melt flow rate of all three polypropylenes was determined at 190 °C and 2.16 kg. In some of the PP composites a maleated PP polymer (Orevac CA 100, Arkema, France, MA content 1.0 wt%, M_n = 25000 g/mol) was used as coupling agent. It was always added in 10 wt% calculated for the amount of wood. Five different lignocellulosic fibers were used as reinforcement, four wood flours (W) and a ground corn cob (CC). Three of the wood flours Arbocel CW 630 (volume average particle size, D[4,3] = 39.6 μm, aspect ratio, AR = 3.5), Filtracel EFC 1000 (D[4,3] = 213.1 μm, AR = 6.8) and Arbocel FT400 (D[4,3] = 171. μm, AR = 12.6) were acquired from Rettenmeier and Söhne GmbH, Germany, while the fourth Lasole 200/150 ((D[4,3] = 280.8 μm, AR = 5.4) from La.So.Le. Est Srl, Italy. All four were soft woods; further information was not supplied by the producer. Thee fifth filler was the heavy fraction of corn cob (D[4,3] = 143.4 μm, AR = 2.3) obtained from Boly Kft., Hungary. Particle size was determined by laser light scattering, while aspect ratio manually from SEM micrographs. The abbreviation used indicates the origin of the fibers (wood, W or corn cob, CC) and ten times their aspect ratio, i.e. corn cob with an aspect ratio of 2.3 is referred to as CC23. The amount of the reinforcement usually changed from 0 to 60 wt%, but sometimes composites could not be processed with the largest fiber content because of technological reasons.

All composites were homogenized in a Brabender W 50 EHT internal mixer at 180 °C, 50 rpm for 10 min. Before composite preparation PLA was dried in vacuum, while the fibers in an air circulating oven (110°C for 4 hours and 105 °C for 4 hours, respectively). The homogenized material was compression molded into 1 mm thick plates at 190 °C on

a Fontijne SRA 100 machine. Tensile testing was done by using an Instron 5566 apparatus at 5 mm/min cross-head speed and 115 mm gauge length. Modulus, tensile strength and elongation-at-break were derived from recorded stress vs. strain traces. Micromechanical deformation processes were followed by acoustic emission (AE) testing carried out with a Sensophone AED 40/4 apparatus. AE experiments were supported by scanning electron microscopy (SEM); micrographs were recorded on fracture surfaces created during tensile testing. Failure mechanism was studied also on model composites by polarization optical microscopy (POM). Thin (about 200 μm) films were compression molded from the composites, fractured by tensile testing and then the broken halves studied in the microscope to determine the mode of failure.

3. RESULTS AND DISCUSSION

Although the actual deformation mechanism depends very much on component properties, we do not discuss individual composites, but rather compare them to each other and look for general conclusions. However, first we address two issues very important for the evaluation of our results: wood properties and composite structure. Subsequently we analyze the main micromechanical deformation processes and ways of their identification and then show the importance of the inherent strength of wood particles in the determination of composite performance. Consequences for practice are briefly pointed out in the final section of the paper.

3.1. Structure

Two structural phenomena must certainly be considered in composites containing short fibers or anisotropic particles: aggregation and orientation. The occurrence and extent of aggregation depends on the relative magnitude of adhesion and shear forces acting in the melt during homogenization, i.e. on the forces attracting and separating the particles, respectively. Very limited aggregation is expected in thermoplastics containing lignocellulosic fibers, and especially wood flour. The adhesion forces among the particles are weak because of the very small surface energy of wood being in the range of 40-50 mJ/m^2. The adhesion of particles depends also on their size, which is quite large, at least 100 μm for fillers used in industrial practice as shown in the experimental section. Considerable aggregation is observed at a size of around 2-3 μm for spherical inorganic particles with much larger surface energy. At large wood content, the association of particles, and especially

for those with larger anisotropy, was shown to occur in wood reinforced composites purely from geometric reasons [29]. However, the forces within the aggregates are quite weak and break very easily. None of the micrographs prepared in this study showed any trace of aggregation or association of the particles and the structure of the composites is quite homogeneous.

Anisotropic particles always orientate during the processing of composites and the extent of orientation strongly influences composite properties. Very strong orientation and a wide orientation distribution with a core-shell structure develop in injection molded specimens. However, our composites were homogenized in an internal mixer and then compression molded to 1 mm thick plates. In this case a core-shell structure does not form, but the fibers tend to align parallel with the plane of the plate. On the other hand, random orientation is expected to develop within this plane as shown also by our optical microscopic study (see later). As a consequence, orientation and orientation distribution are the same in all samples, since they were prepared under identical conditions. As mentioned in the introduction of this section, we carry out the comparative analysis of our results and do not wish to apply them to other processing methods or conditions.

3.2. Wood properties

The general idea of fiber reinforced polymers is that the strong fibers carry the load and the matrix transfers it from one fiber to the other. The idea works quite well if the fibers are oriented in the direction of the load, they are sufficiently long and the adhesion between the components is strong. In wood reinforced polymers the principle has some limitations. The adhesion between the matrix and the polymer is often not too strong and the fibers are quite short. A further problem is that the strength of wood is considerably different along the direction of the elementary fibers and perpendicularly to that. This statement is amply demonstrated by the data collected in Table 1. Tensile specimens were machined from plaques of different wood species and tested in two perpendicular directions. We can see that strength depends very much on the type of wood, but even more on orientation. Tensile strength is in the range of 100 MPa in the length direction and around 10 MPa perpendicularly. Additionally, the strength of the same species changes with weather conditions, time of cutting, geographical location, etc. thus the determination of the inherent strength of wood is difficult even when specimens can be prepared from it. However,

the results presented in Table 1 clearly show that wood particles will break mostly parallel to their axis in composites, if they break at all.

The situation is even more difficult in the case of wood flour used as reinforcement in thermoplastic composites. The source or the species is rarely known, the producer usually makes only a distinction between hard and soft wood; mostly the latter is used in plastics. A further problem is created by the small size of the particles, the direct determination of their inherent strength is practically impossible with simple methods. We must also consider the process of failure here. Fracture is initiated at weak sites or flaws and the number of these changes with size. The number of weak sites and the probability of failure is larger in large than in small particles. Accordingly, the inherent strength of wood particles used as fillers depends also on their particle size distribution. The aspect ratio and the orientation of the fibers also influence the strength of the wood as discussed above, and various deformation and failure processes occur in wood reinforced composites, which complicate the determination of any correlation between fiber and composite strength. As a consequence, a strength value, which is representative for the wood flour used as reinforcement cannot be obtained by direct measurements, indirect methods must be used for this purpose. One of the goals of this work was to develop a method and determine representative strength values for wood fibers used as reinforcements in industrial practice under the given processing conditions.

3.3. Deformation mechanisms

The composition dependence of tensile strength is plotted against wood content in Fig. 1 for PP composites prepared with and without a MAPP coupling agent. At poor adhesion, i.e. in the absence of the coupling agent (F_a ~70 mJ/m^2 [32]), strength mainly decreases with increasing wood content, while improved adhesion (F_a ~ 580 mJ/m^2 [32]) results in a considerable increase in strength. Four fibers were used in this series of experiments (W35, W68, W126, CC23) and the figure clearly shows that particle characteristics influence strength, and differently at good and poor adhesion. However, the effect of adhesion is much more significant than that of particle characteristics in this particular set of experiments. Based on the differences in the composition dependence of strength observed in Fig. 1, we may speculate that dissimilar micromechanical deformation processes may

take place during deformation at poor and good adhesion, but we do not have much indication about the processes themselves. On the other hand, acoustic emission testing and characteristic quantities derived from the results were shown to offer valuable information about these processes [24,25,33-36].

The result of such a test is presented in Fig. 2. The material was a PLA/$CaSO_4$ model composite, in which only a single micromechanical deformation, debonding occurs [37]. Individual acoustic events are indicated by small circles in the figure. We can see that signals start to appear above a critical deformation, and they are grouped closely together in the center of the available deformation range. Unfortunately, it is difficult to derive further information from the distribution of individual signals, thus we plotted also the cumulative number of signals in the figure. The corresponding stress vs. strain trace is also included for reference. The cumulative number of signal trace is an S shaped correlation in this case approaching a saturation value in the final range of deformation. Such traces were assigned to debonding previously and this agrees well with the fact that the only particle related deformation process is debonding in the model composite presented [38]. The cumulative number signal trace also allows us the determination of a critical deformation (ε_{AE}) and stress (σ_{AE}) value, which may offer further information on the dominating deformation process [24,25,31,39].

Cumulative number of signal traces may also take other shapes than the one shown in Fig. 2. Three typical correlations are presented in Fig. 3 for a PLA and for two PP composites. The correlation obtained for the hPP/CC composite is very similar to that presented above (see Fig. 2). The adhesion between PP and wood is rather weak because of the small surface energy of the two components [40]. The large particle size of corn cob facilitates debonding even more thus we must assume that this is the dominating micromechanical deformation process in this composite. The other two traces are more or less similar to each other. The increase in adhesion by the use of a coupling agent resulted in considerable initiation deformation (ε_{AE}) and a continuously increasing trace for the hPP/CC/MAPP composite. We may assume again that the mechanism of deformation changed as a result of improved adhesion. The cumulative number of signal trace increases very steeply for the PLA composite and the number of signals is very large. Steeply increasing traces were

assigned to the fracture of wood particles, both in PP [24,25,31,39] and PLA [29,30] composites. The strength of wood is quite small perpendicularly to fiber axis (see Table 1) and the particles may break quite easily, if their orientation allows it.

The assumption on fiber fracture is strongly corroborated by Fig. 4 showing the polarization optical micrograph taken from a PLA/wood composite film. PLA films containing 5 vol% wood were broken in a tensile testing machine and then studied by POM. The micrograph demonstrates quite well that wood particles fractured along their axis and this fracture led to the failure of the film. Similar micrographs were recorded on composites prepared with other reinforcements like W68 and CC23. Depending on the studied system several local mechanisms were identified also by SEM. In accordance with earlier conclusions mainly debonding takes place in hPP/wood composites (Fig. 5a), while fiber fracture dominates in PLA based materials (Fig. 5b). Obviously, several micromechanical deformations may take place in thermoplastic/wood composites, which can be identified with a large probability by acoustic emission measurements supported by microscopy and the analysis of characteristic stresses supplies even more information about these processes.

3.4. Composite strength

The stress characterizing the initiation of the main deformation process (σ_{AE}) is plotted against wood content for several composites prepared with the corn cob filler (CC23) in Fig. 6. Values obtained for PP composites prepared both with or without a coupling agent are presented in the figure. We see that without coupling (full symbols) the dominating process is initiated at very small stresses and initiation stress depends only slightly on the type of the matrix used. Significantly different correlations are obtained at good adhesion (empty symbols). Characteristic stress increases for PP and decreases somewhat for PLA with increasing fiber content and what is most surprising, the correlations converge on the same final value at wood volume fraction of 1 ($\varphi_w = 1$), i.e. for neat wood, independently of the matrix. This value is 29.2 MPa with ±1.4 MPa standard deviation for the CC23 filler. Exponential correlations were fitted to the experimental points to obtain the lines plotted in Fig. 6 and the value mentioned above. This value must be the inherent strength of this particular wood fiber under the present conditions and it represents the upper limit of strength which can be achieved with these composites.

Inherent strength values and confidence intervals at the 5 % level were calculated

for the different fillers and matrices to check the reliability of our predictions. Additionally, the different sets of data were compared by the Mann-Whitney U test to verify the null hypothesis that the various populations of the results are different or identical. The *p*-value of the statistical test proved to be larger than 0.05 in all cases, which is insufficient to reject the null hypothesis that the inherent strength of the wood is the same in the different matrices at the significance level of 5 %. Accordingly, statistical analysis proved that composite strength is determined by the inherent strength of the fibers indeed and the reliability of the fitting procedure is further corroborated by the small standard deviation of the obtained values, which is quite surprising since extrapolation was done to a distant value.

The procedure was repeated also for the other fibers. The corresponding correlation is presented in Fig. 7 for composites containing one of the wood fibers (W68). The figure is very similar to the previous one (Fig. 6) with the exception that the value extrapolated to the wood volume fraction of 1, is somewhat larger, 33.5±1.1 MPa indicating a larger inherent strength for this lignocellulosic filler. Considering the structure of corn cob and also the fact that the separation of heavy and light fractions is never perfect, this difference and the value is reasonable.

We obtain a slightly different picture when we generate the same plot for the composites prepared with the W36 fiber (Fig. 8). The particle size of this fiber is considerably smaller than those of the other two discussed previously (CC23 and W68) and its aspect ratio is also quite small. The correlations presented in Fig. 8 indicate two different mechanisms depending on the matrix polymer used. The fracture of the particles may occur in hPP/MAPP and PLA composites, the correlations of which converge on each other reaching the strength value of 38.9±1.8 MPa at $\varphi_w = 1$. The smaller particle size of this wood fully justifies this large value (see also discussion in section 3.2). The extrapolated strength of the rPP composites, however, assumes a different, smaller value than the one obtained for the other two series. Obviously, some other factor and not the inherent strength of the particles determines composite strength here. We believe that because of the small size, larger strength and small aspect ratio of the fiber, neither debonding nor particle fracture can take place in these composites, but shear yielding dominates because of the small modulus and yield stress of the matrix.

Similarly complicated are the correlations presented in Fig. 9 for composites containing the relatively long thin fibers of W126. Characteristic stress increases and the same approach of extrapolation can be used at small fiber content, but points measured at larger fiber loadings deviate strongly from the predicted tendency. All deviations are negative, i.e. micromechanical deformations are initiated at smaller stress than expected. In a detailed study of the phenomenon we showed that these fibers associate and form a network above a critical fiber content [29]. The network is relatively weak and fails at small stresses thus initiating cracks in the matrix, which results in the small σ_{AE} values. Characteristic stress obtained by extrapolation, however, is larger here than for the other three fillers (56.1±0.5 MPa). Since the diameter of the fiber is approximately the same as that of the small filler (W35), it cannot fail with the same mechanism, i.e. fracture in the axis direction. Both the larger σ_{AE} value and SEM micrographs indicate that fibers break perpendicularly to their axis in these composites, a conclusion supported also by Fig. 10. Although the debonding of a fiber can also be seen in the middle of the micrograph, at least three or four fibers broken perpendicularly are located at the top of the micrograph (indicated by circles).

3.5. Discussion, consequences

Acoustic emission testing and the analysis of the results obtained on a variety of polymer/wood composites indicate that if adhesion between the matrix and the wood fibers is good, the dominating micromechanical deformation process which initiates the failure of the composites is fiber fracture. However, fibers may fracture parallel or perpendicular to their axis and the stress necessary for fracture depends also on their diameter. This latter statement is confirmed by Fig. 11, in which predicted fiber strength is plotted against the diameter of the fibers. A reasonably close linear correlation is obtained for all fibers tested except one, the thin long fiber with the aspect ratio of 12.6. This latter fails at considerably larger stress than the others, because it breaks perpendicularly to its axis, while the others split in axis direction. The figure confirms also our original assumption that fiber strength depends on particle size; larger particles fail at smaller stress. Fiber failure occurs between 31 and 45 MPa for parallel, while at around 56 MPa for perpendicular fracture.

One may question the importance of inherent fiber strength in composite performance. The tensile strength of the composites is plotted against the initiation stress (σ_{AE})

of the dominating micromechanical deformation process in Fig. 12. The very close correlation and the similar values for strength and σ_{AE} indicate that local deformations initiated around wood particles result in the almost immediate failure of the composite. This proves that the inherent strength of the fiber determines maximum composite strength which can be achieved with the given combination of a fiber and a matrix. The statement is strongly supported by the points located around the upper end of the correlation, which belong to the long thin fibers. Composite strength can be increased only by increasing inherent fiber strength, which may be achieved by the proper selection of fiber characteristics (diameter, aspect ratio), chemical treatment or processing conditions, i.e. the alignment of the fibers.

4. CONCLUSIONS

Acoustic emission measurements and the analysis of results obtained on a considerable number of thermoplastic polymer/wood composites prepared with various matrices and fibers proved that micromechanical deformation processes initiated by the fibers determine the performance of the composites. Debonding usually leads to the decrease of composite strength, but decreasing strength is not always associated with poor adhesion and debonding. The direction of property change with increasing wood content depends on component properties and interfacial adhesion. Good interfacial adhesion of the components often results in the fracture of the fibers in polymer/lignocellulosic fiber composites. Depending on their size and aspect ratio fibers may fracture parallel or perpendicular to their axis. At good adhesion the maximum strength achieved for a particular polymer/wood pair depends on the inherent strength of the fibers, which is larger for perpendicular than parallel fracture. Inherent fiber strength effective in a composite depends also on particle size, larger particles fail at smaller stress, because of the larger number of possible flaws in them. A very close correlation exists between the initiation stress of the dominating local deformation process and composite strength proving that these processes lead to the failure of the composite and determine its performance.

5. ACKNOWLEDGEMENTS

The authors are indebted to Zsolt László for his help in the determination of the particle characteristics of wood and for Ágnes Gábor, Gábor Dora, and Áron Csikós for

the preparation of composite samples. The research on heterogeneous polymer systems was financed by the National Scientific Research Fund of Hungary (OTKA Grant No. K 101124) and by the Forbioplast FP7 project of EU (212239); we appreciate the support very much. One of the authors (KR) is grateful also to the János Bolyai Research Scholarship of the Hungarian Academy of Sciences.

6. REFERENCES

[1] Foster C., Hackwell B., Pritchard G. Wood-plastic composite growth taking off in Europe. Additives for Polymers. 2006;2006(5):9-10.

[2] Carus M, Gahle C, Korte H. Market and future trends for wood polymer composites in Europe: the example of Germany. In: Oksman K, Sain M, editors. Wood-polymer composites, Boca Raton: CRC Press LLC; 2008. p. 300-330.

[3] Markarian J. Additive developments aid growth in wood-plastic composites. Plastics, Additives and Compounding. 2002;4(11):18-21.

[4] Bledzki AK, Gassan J, Theis S. Wood-filled thermoplastic composites. Mech Compos Mater. 1998;34(6):563-568.

[5] Bax B, Müssig J. Impact and tensile properties of PLA/Cordenka and PLA/flax composites. Compos Sci Technol. 2008;68(7-8):1601-1607.

[6] Huda MS, Mohanty AK, Drzal LT, Schut E, Misra M. "Green" composites from recycled cellulose and poly(lactic acid): Physico-mechanical and morphological properties evaluation. J Mater Sci. 2005;40(16):4221-4229.

[7] Huda MS, Drzal LT, Misra M, Mohanty AK. Wood-fiber-reinforced poly(lactic acid) composites: Evaluation of the physicomechanical and morphological properties. J Appl Polym Sci. 2006;102(5):4856-4869.

[8] Plackett D, Lřgstrup Andersen T, Batsberg Pedersen W, Nielsen L. Biodegradable composites based on -polylactide and jute fibres. Compos Sci Technol. 2003;63(9):1287-1296.

[9] Sreekumar PA, Thomas S. Matrices for natural-fibre reinforced composites. In: Pickering KL, editor. Properties and performance of natural-fibre composites, Boca Raton: Woodhead Publishing; 2008. p. 67-126.

[10] Oksman K, Skrifvars M, Selin J-F. Natural fibres as reinforcement in polylactic acid (PLA) composites. Compos Sci Technol. 2003;63(9):1317-1324.

[11] Mathew AP, Oksman K, Sain M. Mechanical properties of biodegradable composites from poly lactic acid (PLA) and microcrystalline cellulose (MCC). J Appl Polym Sci. 2005;97(5):2014-2025.

[12] Markarian J. Wood-plastic composites: current trends in materials and processing. Plastics, Additives and Compounding. 2005;7(5):20-26.

[13] Staiger MP, Tucker N. Natural-fibre composites in structural applications. In: Pickering KL, editor. Properties and performance of natural-fibre composites, Boca Raton: Woodhead Publishing; 2008. p. 269-300.
[14] Tichy RJ. Performance measurement and construction applications of wood-polymer composites. In: Oksman K, Sain M, editors. Wood-polymer composites, Boca Raton: CRC Press LLC; 2008. p. 259-272.
[15] Stark NM, Rowlands RE. Effects of wood fiber characteristics on mechanical properties of wood/polypropylene composites. Wood Fiber Sci. 2003;35(2):167-174.
[16] Ichazo MN, Albano C, Gonzalez J, Perera R, Candal MV. Polypropylene/wood flour composites: treatments and properties. Compos Struct. 2001;54(2-3):207-214.
[17] Selke SE, Wichman I. Wood fiber/polyolefin composites. Composites Part A. 2004;35(3):321-326.
[18] Bledzki AK, Jaszkiewicz A. Mechanical performance of biocomposites based on PLA and PHBV reinforced with natural fibres - A comparative study to PP. Compos Sci Technol. 2010;70(12):1687-1696.
[19] Raj RG, Kokta BV, Daneault C. Effect of chemical treatment of fibers on the mechanical properties of polyethylene-wood fiber composites. J Adhes Sci Technol. 1989;3(1):55-64.
[20] Borja Y, Rieß G, Lederer K. Synthesis and characterization of polypropylene reinforced with cellulose I and II fibers. J Appl Polym Sci. 2006;101(1):364-369.
[21] Yang H-S, Wolcott MP, Kim H-S, Kim S, Kim H-J. Effect of different compatibilizing agents on the mechanical properties of lignocellulosic material filled polyethylene bio-composites. Compos Struct. 2007;79(3):369-375.
[22] Nachtigall SMB, Cerveira GS, Rosa SML. New polymeric-coupling agent for polypropylene/wood-flour composites. Polym Test. 2007;26(5):619-628.
[23] Goodier JN. Concentration of stress around spherical and cylindrical inclusions and flaws. J Appl Mech. 1933;55:39-44.
[24] Renner K, Móczó J, Pukánszky B. Deformation and failure of PP composites reinforced with lignocellulosic fibers: Effect of inherent strength of the particles. Compos Sci Technol. 2009;69(10):1653-1659.
[25] Renner K, Móczó J, Suba P, Pukánszky B. Micromechanical deformations in PP/lignocellulosic filler composites: Effect of matrix properties. Compos Sci Technol. 2010;70(7):1141-1147.
[26] Hristov VN, Lach R, Grellmann W. Impact fracture behavior of modified polypropylene/wood fiber composites. Polym Test. 2004;23(5):581-589.
[27] Hristov VN, Vasileva ST, Krumova M, Lach R, Michler GH. Deformation mechanisms and mechanical properties of modified polypropylene/wood fiber composites. Polym Compos. 2004;25(5):521-526.
[28] Guo C-g, Wang Q-w. Effect of maleic anhydride grafted styrene-ethylene-butylene-styrene

(MA-SEBS) on impact fracture behavior of polypropylene / wood fiber composites. J Forestry Res. 2007;18(3):203-207.

[29] Faludi G, Hári J, Renner K, Móczó J, Pukánszky B. Fiber association and network formation in PLA/lignocellulosic fiber composites. Compos Sci Technol. 2013;77(0):67-73.

[30] Faludi G, Dora G, Renner K, Móczó J, Pukánszky B. Biocomposite from polylactic acid and lignocellulosic fibers: Structure-property correlations. Carbohydr Polym. 2013;92(2):1767-1775.

[31] Renner K, Kenyó C, Móczó J, Pukánszky B. Micromechanical deformation processes in PP/wood composites: Particle characteristics, adhesion, mechanisms. Composites Part A. 2010;41(11):1653-1661.

[32] Renner K, Móczó J, Vörös G, Pukánszky B. Quantitative determination of interfacial adhesion in composites with strong bonding. Eur Polym J. 2010;46(10):2000-2004.

[33] Bohse J. Acoustic emission characteristics of micro-failure processes in polymer blends and composites. Compos Sci Technol. 2000;60(8):1213-1226.

[34] Kraus R, Wilke W, Zhuk A, Luzinov I, Minko S, Voronov A. Investigation of debonding processes in particle-filled polymer materials by acoustic emission: Part I Acoustic emission and debonding stress. J Mater Sci. 1997;32(16):4397-4403.

[35] Kraus R, Wilke W, Zhuk A, Luzinov I, Minko S, Voronov A. Investigation of debonding processes in particle-filled polymer materials by acoustic emission: Part II Acoustic emission amplitude and energy release by debonding. J Mater Sci. 1997;32(16):4405-4410.

[36] Czigány T, Marosfalvi J, Karger-Kocsis J. An acoustic emission study of the temperature-dependent fracture behavior of polypropylene composites reinforced by continuous and discontinuous fiber mats. Compos Sci Technol. 2000;60(8):1203-1212.

[37] Imre B, Keledi G, Renner K, Móczó J, Murariu M, Dubois P, et al. Adhesion and micromechanical deformation processes in PLA/$CaSO_4$ composites. Carbohydr Polym. 2012;89(3):759-767.

[38] Renner K, Yang MS, Móczó J, Choi HJ, Pukánszky B. Analysis of the debonding process in polypropylene model composites. Eur Polym J. 2005;41(11):2520-2529.

[39] Dányádi L, Renner K, Móczó J, Pukánszky B. Wood flour filled polypropylene composites: Interfacial adhesion and micromechanical deformations. Polym Eng Sci. 2007;47(8):1246-1255.

[40] Maldas D, Kokta BV. Interfacial adhesion of lignocellulosic materials in polymer composites: an overview. Compos Interfaces. 1993;1(1):87-108.

Table 1 Tensile strength of wood specimens in directions relative to the orientation of the fibers

Wood	Tensile strength (MPa)	
	parallel	perpendicular
spruce	81.6 ± 17.7	3.8 ± 0.8
oak	105.9 ± 13.4	13.4 ± 0.6
ash	159.9 ± 27.7	12.7 ± 1.1

7. CAPTIONS

Fig. 1 Effect of wood content, fiber characteristics and adhesion on the tensile strength of hPP/wood composites. Symbols: (○,●) CC23, (▽,▼) W35, (△,▲) W68, (□,■) W126; full symbols: without coupling (poor adhesion), empty symbols: with MAPP (good adhesion).

Fig. 2 Results of the acoustic emission testing of a PLA/$CaSO_4$ model composite containing 15 vol% filler. Small circles indicate individual signals; the S shape curve is the cumulative No. of signal trace. The stress vs. strain correlation is added for reference.

Fig. 3 Comparison of the cumulative No. of signal traces of three typical polymer/lignocelluslosic fiber composites. Fiber: 20 vol% CC. ——— hPP, ----- hPP+MAPP, ····· PLA.

Fig. 4 Fracture of the fiber in a PLA/wood (5 vol% W54) model composite film. Polarization optical micrograph.

Fig. 5 Micromechanical deformation processes in polymer/wood composites; a) extensive debonding and plastic deformation of the matrix in hPP/wood (20 vol% W126), b) fiber fracture in PLA/wood (20 vol% W68) composites, respectively.

Fig. 6 Composition dependence of the characteristic stress determined by acoustic emission for composites prepared with the CC23 fiber. Extrapolation to $\varphi_w = 1$. Full symbols indicate PP composites with poor adhesion (no MAPP).

Fig. 7 Effect of wood content on σ_{AE} for composites containing W68. Extrapolation to 100 % wood content.

Fig. 8 Dependence of initiation stress on wood content and the type of matrix for composites prepared with the W35 fiber. Extrapolation to $\varphi_w = 1$. Change of deformation mechanism in rPP (▽) composites.

Fig. 9 Effect of wood content and matrix type on the characteristic stress of the dominating micromechanical deformation process for composites containing W126. Extrapolation and additional mechanism related to the failure of the fiber network.

Fig. 10 SEM micrograph recorded on the fracture surface of a PLA/wood (20 vol % W126) composite. Fracture of the fibers perpendicularly to their axis.

Fig. 11 Effect of fiber diameter on the inherent strength of wood in polymer/wood composites.

Fig. 12 Close correlation between the initiation stress of the dominating deformation process and the strength of the composite. Symbols: PLA: (◓, ◑, ◒, ○, ●), rPP: (▲, ◭, ◬, △, ▲), hPP: (⬒, ◨, ⬓, □, ■), CC23: (◓, ▲, ⬒), W35: (◑, ◭, ◨), W54 (◒, ◬, ⬓), W68 (○, △, □), W125 (●, ▲, ■)

Faludi, Fig. 1

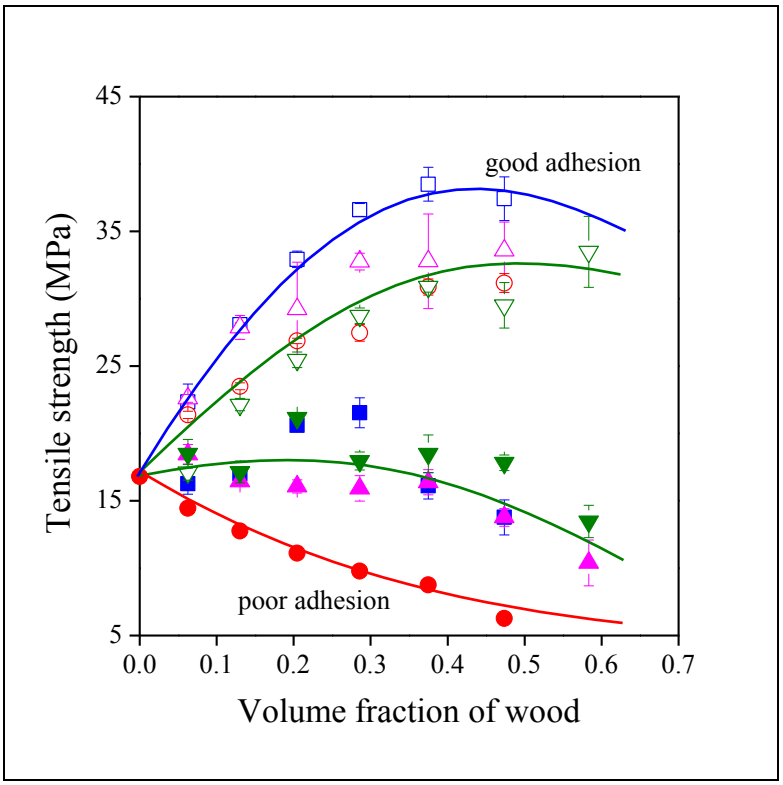

Faludi, Fig. 2

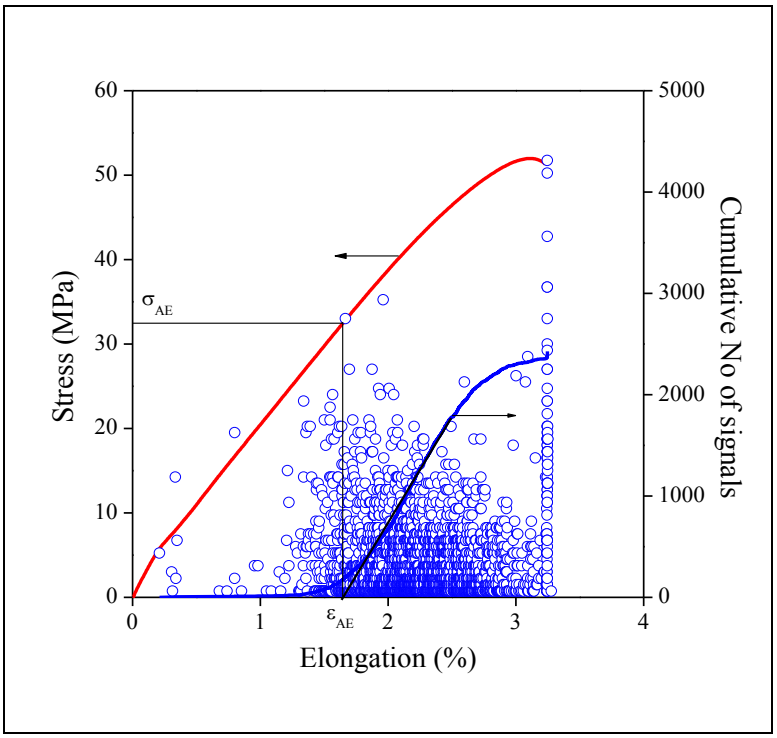

Faludi, Fig. 3

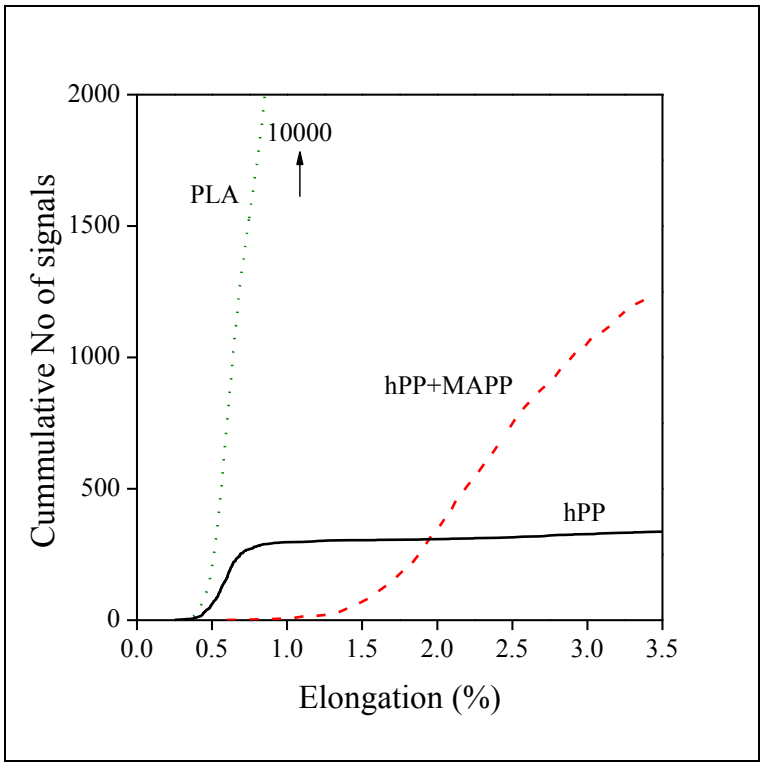

Faludi, Fig. 4

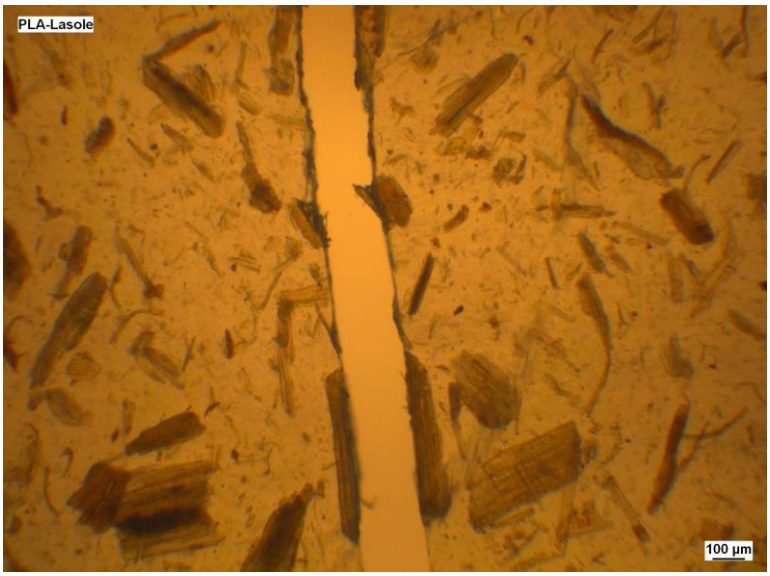

Faludi Fig. 5

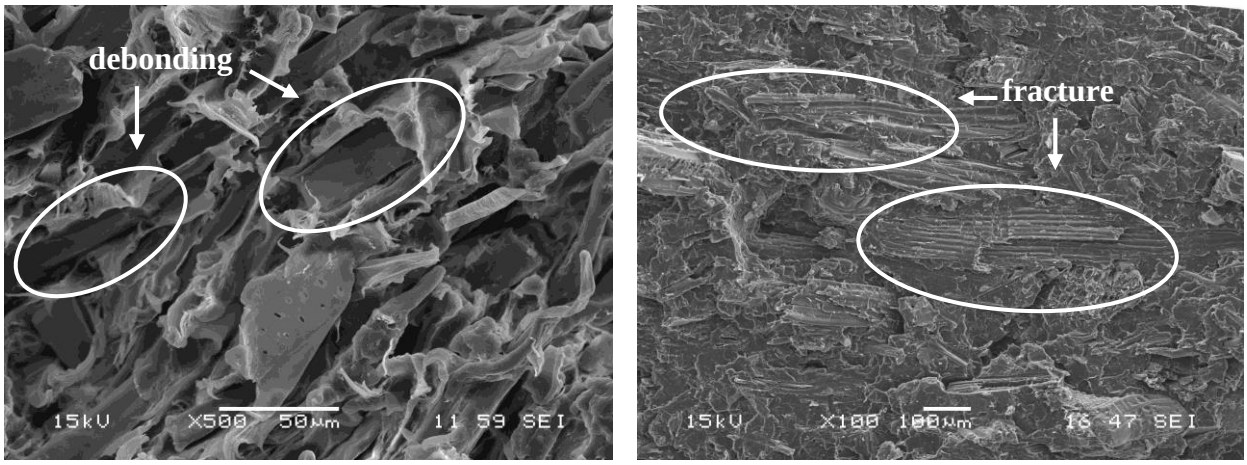

a) b)

Faludi, Fig. 6

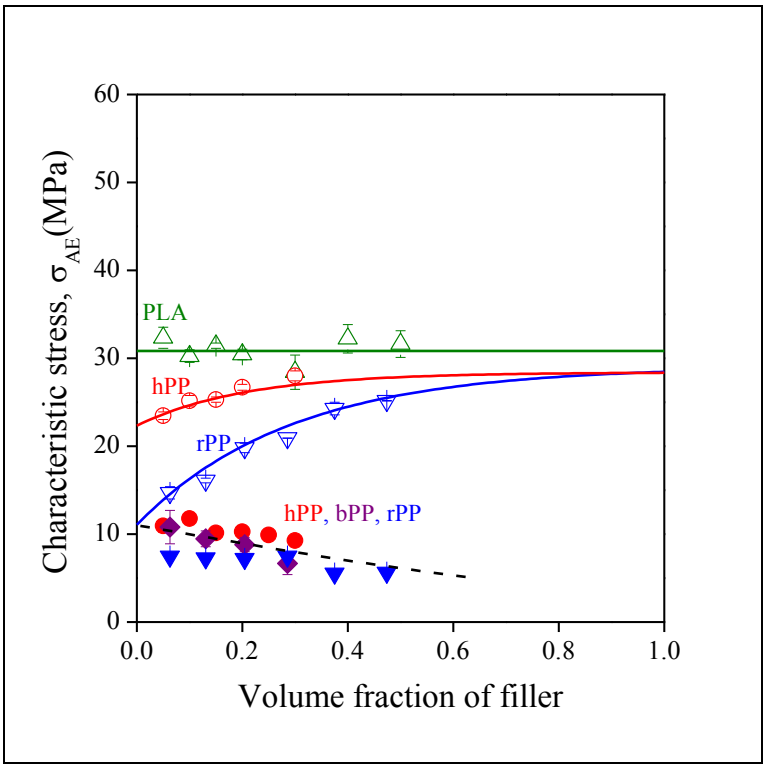

Faludi, Fig. 7

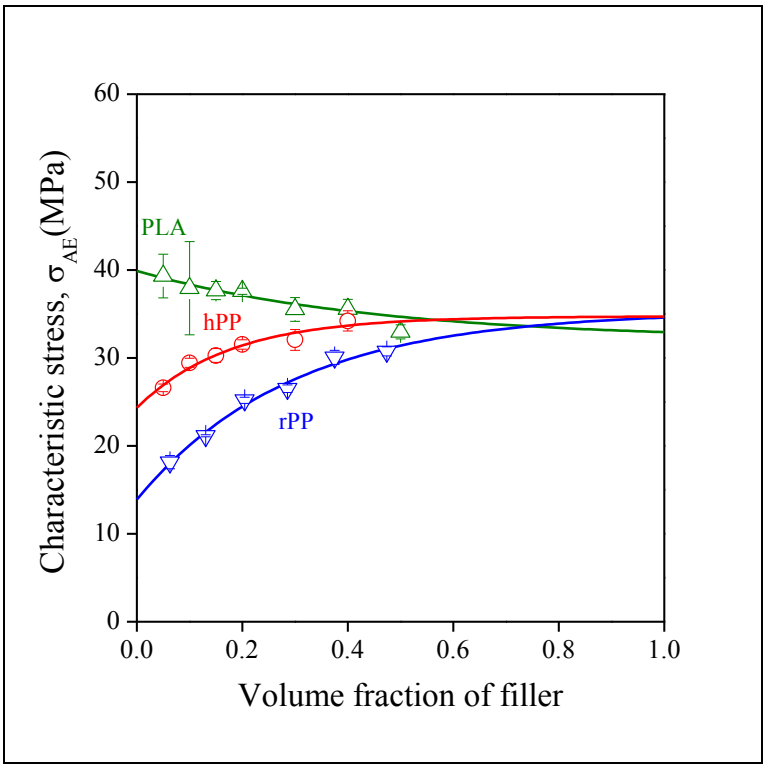

Faludi, Fig. 8

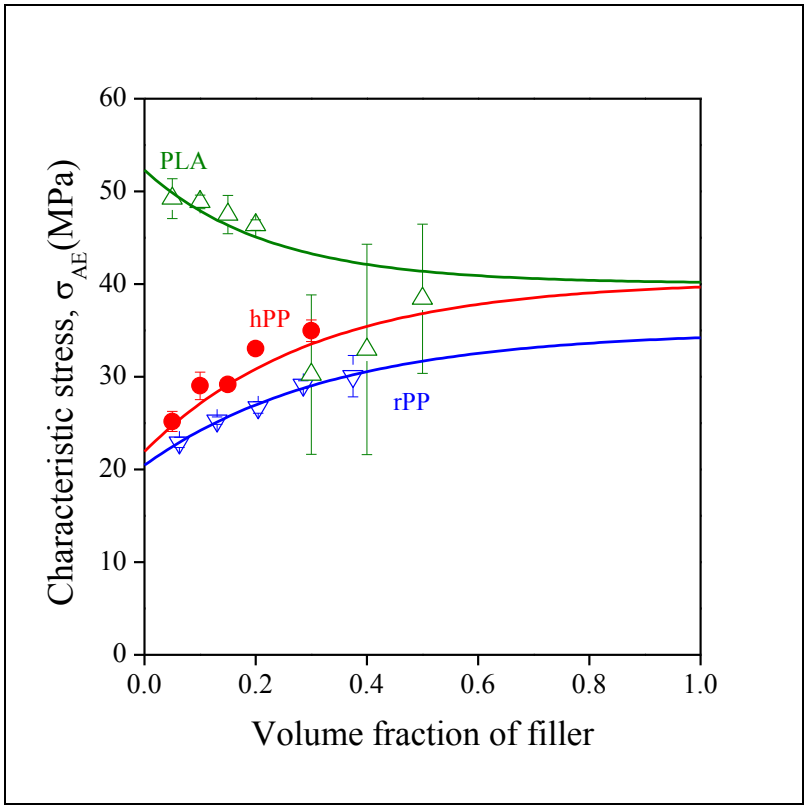

Faludi, Fig. 9

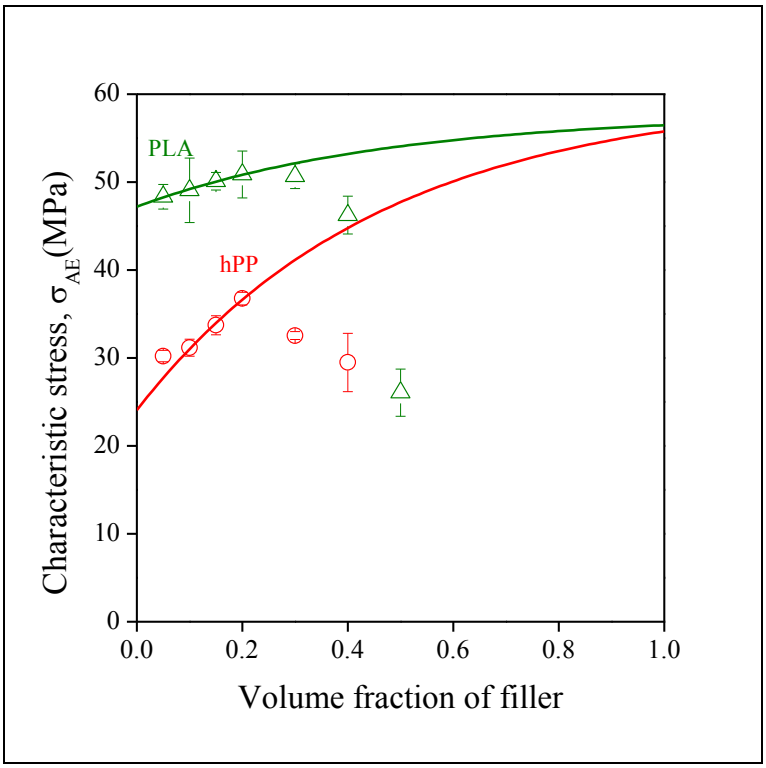

Faludi, Fig. 10

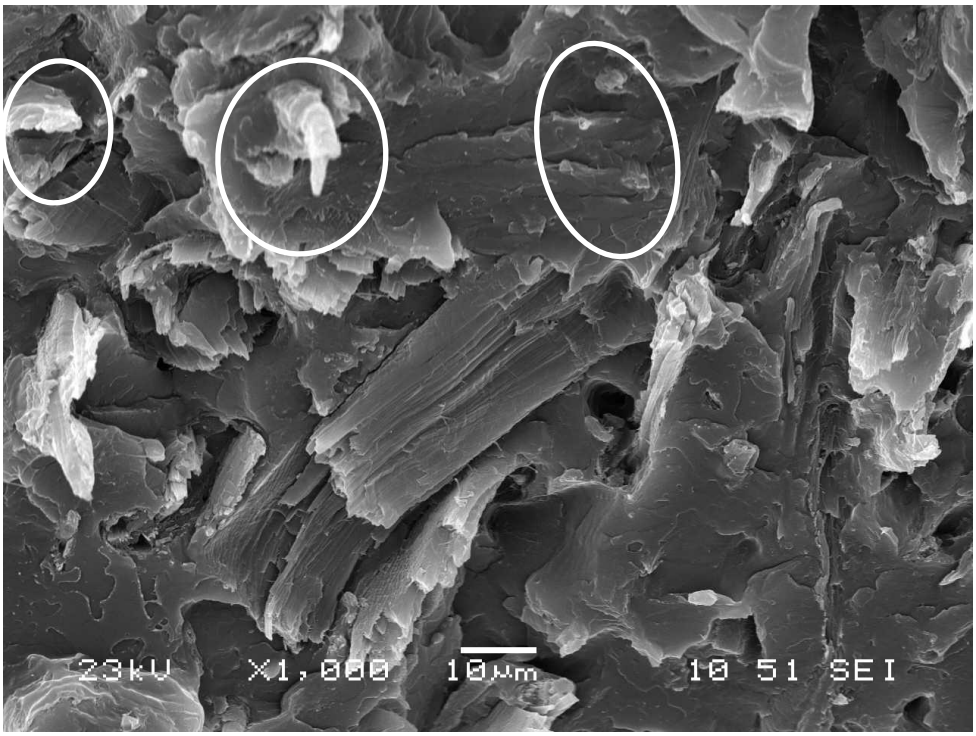

Faludi, Fig. 11

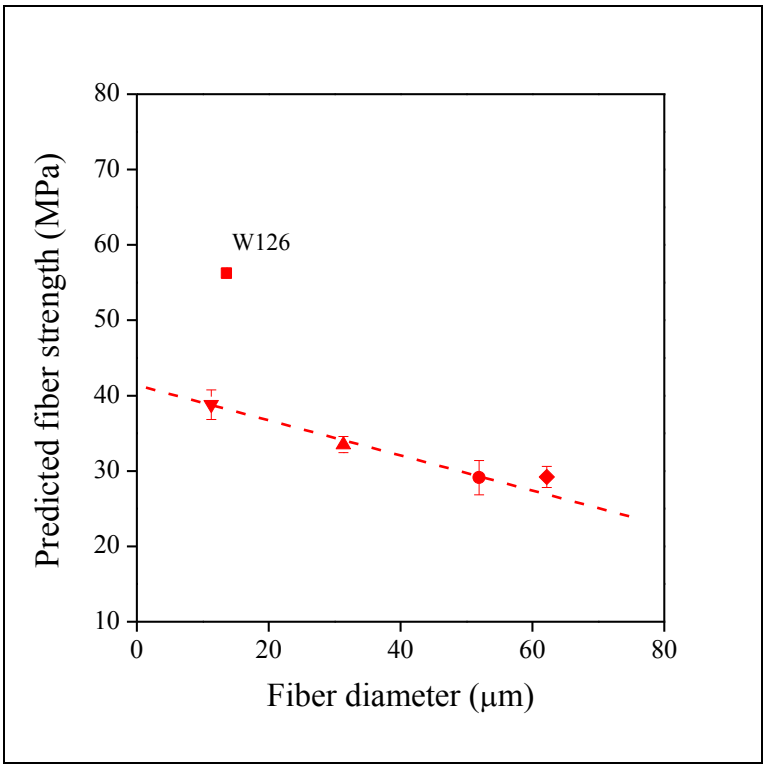

Faludi, Fig. 12